JOURNAL OF MATERIALS SCIENCE 14 (1979) 2373–2383

The behaviour of boron–aluminium composites during and after impact

G. RICH, A. R. BUNSELL
Ecole Nationale Supérieure des Mines de Paris, Centre des Matériaux, BP 87, 91003 Evry Cédex, France

The behaviour of two types of aluminium alloy (1200 and 2024) reinforced unidirectionally by boron fibres has been studied and the effect of an impact on the residual properties and under fatigue conditions determined. Spherical and cylindrical indenters have been used over a range of speeds covering six orders of magnitude. It is found that the fibres fail due to bending induced by the impact, but that the matrix surrounding the breaks is not necessarily cracked. The tensile strengths of impacted specimens have been compared to strengths of similar specimens containing a partial surface notch, simulating the impact damage, and good agreement found. Impacted specimens have been tested in circular bending fatigue on a machine which has been developed so as to maintain the maximum applied load constant despite any change of specimen compliance. The matrix bridge is quickly broken under cyclic loading and the B-2024 specimens show signs of progressive fibre damage. The *S–N* curve for the B-1200 specimen is much flatter due to the inability of the softer matrix to transmit high stresses to fibres neighbouring fibre breaks. The residual tensile strength of impacted boron–aluminium is found to depend on the remaining intact fibres and not on the matrix. In fatigue the notch effect produced by the damage zone is reduced at long lifetimes as cracking of the matrix parallel to the fibres isolate the damaged region.

1. Introduction

Boron fibres have to a great extent been eclipsed by carbon fibres as the reinforcing agent for many composite applications, but as a reinforcement for metal matrix composites they remain largely unchallenged, as they have exceptionally high specific properties. There are considerable advantages in having a metal matrix in comparison with the alternative of a resin as the matrix for a composite; for example, it is inherently stronger and hence the transverse properties of the composite are higher. In addition metals can be taken to higher temperatures than is at present possible with organic matrix materials. Although an aluminium matrix is less brittle and so tougher than the commonly used organic matrix materials, it has been known for some considerable time that one of the major problems for the use of all high performance composite materials is their fragility under impact. Due to their high intrinsic cost boron fibres are mainly attractive for applications for which their specific properties are a more important consideration than initial cost. This obviously means that the aerospace industry is a potential user of this material, and for many of the applications in this domain the problem of impact is paramount.

There are several interesting studies of the failure by impact of resin-based composites such as those of Husmann [1], who showed that for carbon and glass fibre composites the damage caused by an impact depended on the properties of the fibre and not the resin. This study indicates that to obtain a high fracture energy, fibres of high strength but low modulus should be used. Oplinger and Slepetz [2] have studied the effect of shock and also slow penetration of an impacter on CFRP and GRP and found that the damage prod-

0022–2461/79/102373–11 $03.10/0

uced increases with a decrease of fibre breaking strain.

Harris and Bunsell [3] examined the impact properties of glass/carbon fibre hybrid composites and found that the energy absorbed in a Charpy test was the sum of the energies absorbed by each composite component measured independently.

Butcher [4] has described experiments in which specimens of CFRP or GRP were placed on a support of lead and impacted. The shape of the impacter at the point of contact was cylindrical. This study showed that delamination at the fibre–matrix interface, which served to isolate the impact damage, was favoured by the use of high strength fibres and weak interfaces.

Jacques [5] and Carlisle [6] have compared the residual strengths of the aluminium alloy 6061 reinforced by boron fibres after impact by both rubber and steel balls with the strengths of the titanium alloy T1 6 wt% A1 4 wt% V impacted in a similar manner. They showed that the composite material was much more sensitive to impact than the titanium alloy, and that its residual strength falls with impact energy until a minimum is reached when the material is perforated. These authors showed that the residual strength of the composite was increased by fatigue loading which produced cracks parallel to the fibre direction.

The energy absorbed during the Charpy test of boron fibre unidirectionally reinforced alloys has been shown [7] to increase with fibre volume fraction, the diameters of the fibres and with a reduction of yield strength of the matrix. The method of fabrication of the composite was also shown to influence the energy absorbed.

It has been suggested in a study by Awerbuch and Hahn [8] that the impact energy is partially dissipated by the creation of new fracture surfaces in the impact zone. Their studies for pure aluminium reinforced by boron fibre (B–Al) and titanium reinforced by silicon carbide coated boron fibres (BorSiC/Ti) produced no correlation between the energy of the impact or the size of the damaged zones and the fracture energy of the composite calculated from the results of tensile tests. The effects of the impacts were found to be much less with the titanium composite than with the aluminium composite.

Studies of the fatigue properties of B–Al by Gray [9] who tested his specimens in circular bending, in which a constant moment is applied to the pivoted grips, have suggested that impact damaged specimens have better properties than undamaged specimens.

Greszczuk [10] has adapted the Hertzian theory of contact for orthotropic material and has calculated the stresses produced in the target material which is being impacted. This study has shown that the momentum necessary to produce initial degradation of the material increases with an increase in tensile strength of the composite, whilst an increase in elastic modulus and hence fragility has the reverse effect.

Even after the studies mentioned above the impact behaviour and the mechanisms involved in this type of damage of B–Al are not well defined, particularly in situations relating closely to those likely to be encountered in reality. It is towards this end that this work has been directed and has involved a study of the controlling mechanisms involved in the damage by impact of B–Al, measurements of residual strengths and the behaviour of the impacted material in a realistic fatigue situation.

2. Material tested

Two types of matrix material have been considered in this study, industrially pure aluminium (1200) and an aluminium alloy with the American designation 2024. The boron fibres were obtained from Composite Material Corporation, USA, and were of 100, 142 and 200 μm diameter. The boron fibres were filament-wound onto a drum and glued together by a projection of polystyrene, which permits a sheet of aligned fibres to be removed from the drum. Plates of B–Al were then made by sandwiching the fibres between sheets of the matrix material. This sandwich structure was then hot-pressed under vacuum at a temperature and pressure which depended on the matrix material and which produced diffusion bonding. The polystyrene was removed during this process during a period of out-gassing. The volume fraction normally chosen to be 55% is controlled by the thickness of the sheets of matrix material and the gauge spacing of the fibres. Table I gives details of the manufacturing conditions for the material used in this study, as well as the dimensions of the flat rectangular specimens which were tested.

In order to control the state of the 2024 alloy the composite was heat-treated for 20 min at 495° C after manufacture and then quenched in

TABLE I Average pressure $\bar{p}$ for plastic flow of the matrix showing large differences between the values obtained from the load–penetration curves and the dimension of the imprint

Material	$H_{V_{2000}}$ microhardness number with 200 g load	Using curves of slow penetration $\bar{p}$ (MPa)	Using dimensions of imprint $\bar{p}$ (MPa)
B-1200	2–2.4	220	5.4–6.1
B-2024-T4	13.9	770	19–20

water at room temperature. The specimens were left at room temperature for a minimum of four days after heat treatment before being tested.

3. Experimental methods

Mechanical tensile tests and others involving slow penetration of a projectile were conducted on a 10 t capacity Instron tensile machine. The specimen was placed on a flat steel support attached to the cross beam of the Instron. Two types of penetrators have been used, one hemispherical of diameter 6 mm and the other semi-cylindrical of diameter 5 mm and length 12 mm, so providing regular and controlled contact surfaces. An acoustic emisson transducer coupled to the steel block allowed events which produced emissions to be recorded. The loads applied were measured by an Instron tensile cell and the extension by means of an extensometer. Fig. 1 shows a typical loading and unloading curve obtained together with the acoustic emissions recorded. The energy absorbed by irrecoverable deformation of the matrix produces the hysteresis effects.

In addition an instrumented impact machine has been developed consisting of a steel projectile 10 mm wide and having a semi-cylindrical leading edge of diameter 5 mm. The loading involved during impact is measured by semiconductor strain gauges attached to the projectile 3 mm from the point of contact with the specimen which rested on a support of maraging steel. A static calibration of the machine was made and the band width of the measuring system was greater than 500 kHz. The signal was stored on the oscilloscope with a memory facility.

A fatigue machine has also been developed which cyclically tests rectangular specimens in circular bending and to a constant maximum load even though degradation may cause the compliance of the specimen to vary. The apparatus is shown schematically in Fig. 2. The load on the specimen is transmitted by means of four chains which engage on the sprocket wheels fixed firmly to the grips of the machine which hold the specimen. Using the classical beam formula

$$2\frac{\sigma}{B} = \frac{M}{I} \qquad (1)$$

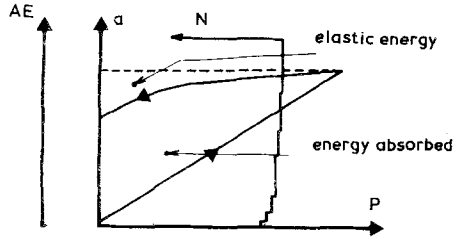

Figure 1 Load–penetration curve and acoustic emission from slow indentation test.

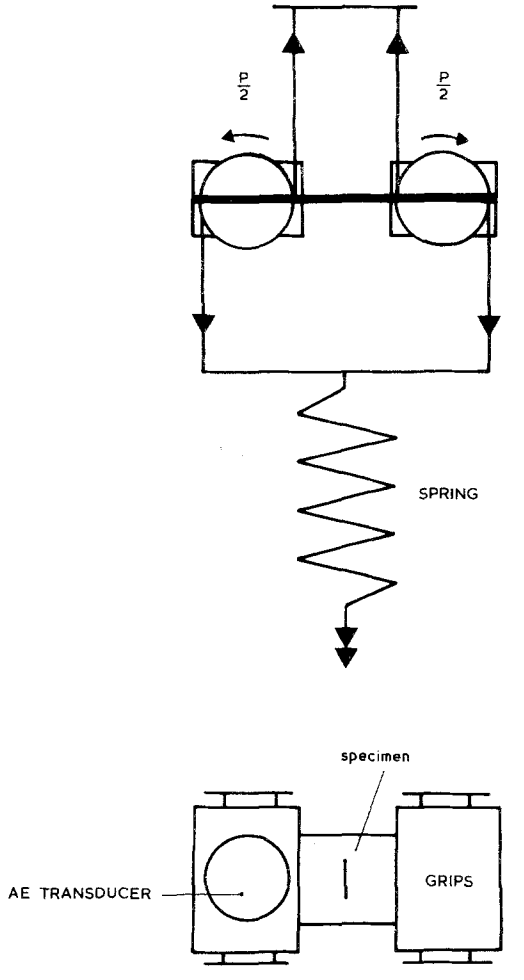

Figure 2 Schematic view of the bending fatigue apparatus.

where σ is the maximuim tensile stress in the beam, B is the thickness, I is the second moment of area of the beam and M is the turning moment applied to the beam we can write for the elastic case considered:

$$\sigma = \frac{6M}{B^2W} = \frac{3dP}{B^2W} \qquad (2)$$

where P is the tension applied to the chains and d is the diameter of the sprocket.

The loading of the system takes place through a spring of high compliance by means of a rigid arm pivoted at the end not attached to the spring and which is then driven through an eccentric cam by an electric motor. The compliance (C) of the spring was 1.3 mm kg^{-1} and the compliance (c) of the system and specimen was typically 0.11 mm kg^{-1}.

As the deflection (D) of the machine was constant we can write

$$D = (C + c)P$$

if the compliance c changes by δc because of damage to the specimen we can write

$$\frac{\delta P}{F} = \frac{-\delta c}{C+c} = \frac{-c}{C+c} \times \frac{\delta c}{c}.$$

Then the variation of load (δF) varies as the ratio of the variation of compliance

$$\left|\frac{\delta P}{P}\right| = \frac{c}{C}\left|\frac{\delta c}{c}\right| \qquad (3)$$

As the variation of compliance of the specimen is rarely more than 10% we can calculate the maximum variation to the load (F) applied using the values of compliances for the system which are given above:

$$\frac{\delta F}{F} = \frac{0.11}{1.3} \times 0.1 \times 100 \approx 1\%.$$

This type of circular bending fatigue machine maintains constant the maximum load applied to the specimen, even if its compliance changes, to within 1%. The frequency of loading with this apparatus was 6 Hz and $\delta_{min}/\delta_{max} = 0.2$.

In addition to the mechanical testing equipment a Dunegan–Endevco acoustic emission (AE) system was used to detect stress wave emissions resulting from failure events in the material. Boron fibres are much bigger in diameter (140 μm) than most other fibres, cf. a carbon fibre has a typical diameter of 7 μm, and are also elastic. Their rupture therefore liberates a great deal of energy which is discernible by the amplitude of the stress wave produced. In these tests a gain of 60 dB or less has been used which allowed the detection of fibre breaks and important sudden fractures of the matrix. The AE transducer was either coupled directly to the specimen by silicone grease, as in the case of the slow impact tests, or to the pivoted grips in the fatigue experiments.

Other means of examination employed were optical and scanning electron microscopy and X-ray radiography.

4. Impact results

Fig. 3 shows the load displacement curves for the slow penetratation of the 6 mm diameter steel ball into the specimen one each of B-1200 and B-2024.

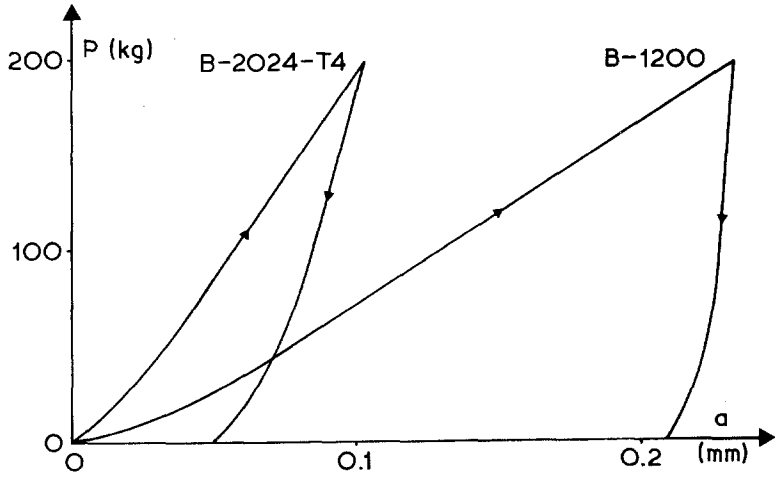

Figure 3 Load–penetration curves for slow indentation.

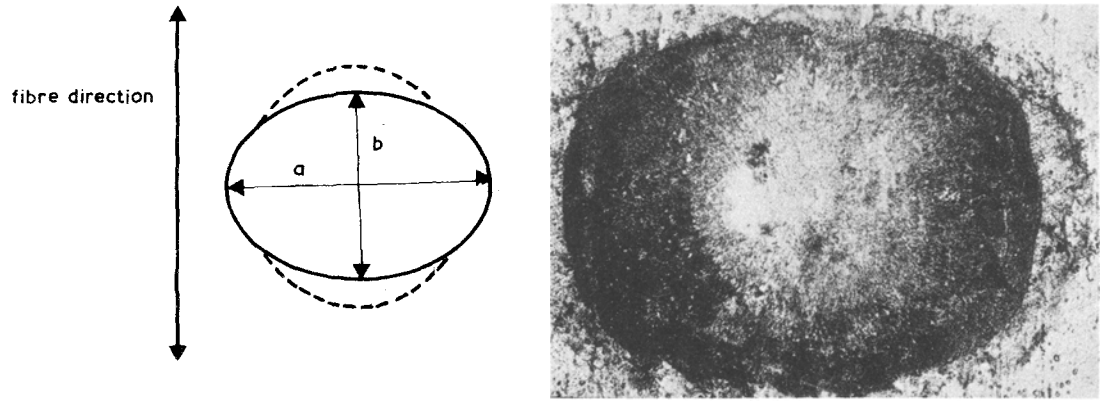

Figure 4 Imprint left in B-2021 after slow penetration test with a 6 mm diameter steel sphere.

In both cases the behaviour is similar to the situation considered in the microhardness test. After yield the penetration is linearly related to the load applied. The flow of the matrix material can be characterized by an average pressure $(\bar{p})$ such that

$$P = 2\pi R\,(\bar{p})\,(\alpha) \qquad (4)$$

in which R is the radius of the sphere and α is the depth of penetration.

There are two ways of determining $\bar{p}$, either by the dimensions of the imprint left by the indenter, as in the microhardness test or by referring to the curves of penetration. As can be seen in Table I the results of these two approaches are not in good agreement and the reason for this may be seen from the form of the imprint obtained which is shown in Fig. 4. Whereas indentations in the unreinforced matrix material are circular in shape, indentations in the composites are elliptical because of the restraining influence of the fibres which are aligned parallel to the minor axis of the ellipse. The ratio of major (a) to minor axis (b) for different composites with a loading of 100 kg is shown in Table II. The presence of the boron fibres means that a greater contact pressure is necessary to produce plastic deformation of the matrix than is the case in the non-reinforced matrix material, as is shown in Fig. 5. In addition fractographic studies have revealed that deformation of the material is not only confined to the impinged zone but extends some way outside this region. In addition the determination of $(\bar{p})$ by the penetration curves include the elastic deformation of the contact zone, which is not entirely negligible in the case of B-2024.

These disparities did not occur with the cylindrical indenter as the loading occurs along a line or strip of material, and in these experiments this was perpendicular to the fibre direction. The pressure needed to produce plastic deformation was increased compared to that necessary for a spherical indenter as the plastic deformation of the matrix in the transverse direction was no longer possible. Table III gives the values obtained. If it is assumed that there is an equivalence of the mechanisms involved, these slow penetration tests permit the behaviour of the material under impact

TABLE II Ratio of major (a) to minor (b) axis of the imprints made with the 6 mm diameter spherical indenter.

	B(100 μm) 1200	B(100 μm) 1200	B(200 μm) 1200	B(142 μm) 2024-T4
$\frac{a}{b}$	1.58	1.38	1.24	1.12

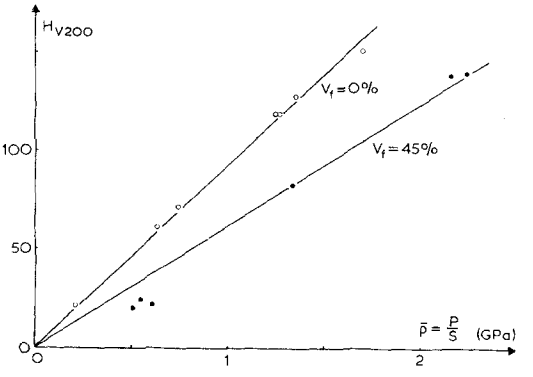

Figure 5 Force to obtain plastic deformation of the matrix as a function of the microhardness.

TABLE III Pressure to obtain plastic flow using a cylindrical penetrator.

	$B(100\,\mu m)$ 1200	$B(142\,\mu m)$ 1200	$B(200\,\mu m)$ 1200	$B(142\,\mu m)$ 2024-T4
$\bar{P}$ (GPa)	0.86	0.84	0.68	2.24

conditions to be calculated by a classical mechanical treatment.

The energy absorbed by the composite during the penetration tests is shown in Figs. 6 and 7 as a function of the maximum loads for the two types of penetrators used.

During the impact experiment the use of the instrumented impact tester permitted a range of speeds which covered six orders of magnitude from 2×10^{-3} mm sec^{-1} for slow penetration to 4×10^{3} mm sec^{-1} for the instrumented impact tests. The pressures $\bar{p}$ calculated for instrumented impact tests were almost identical to those found for the slow indentation in conformity with the

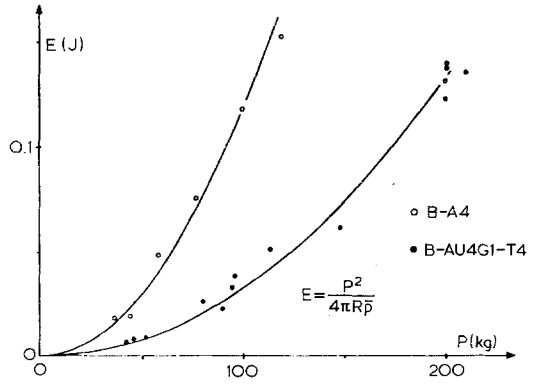

Figure 6 Energy absorbed during penetration as a function of the load applied to the spherical indenter.

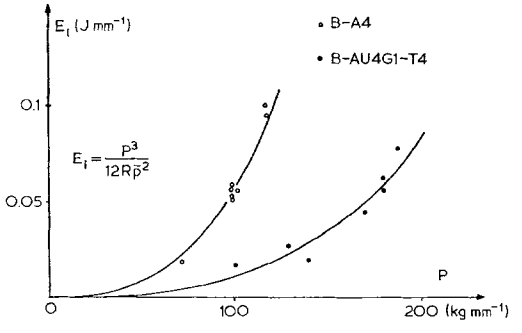

Figure 7 Energy absorbed furing penetration as a function of the load applied per unit length of the semi cylindrical indenter.

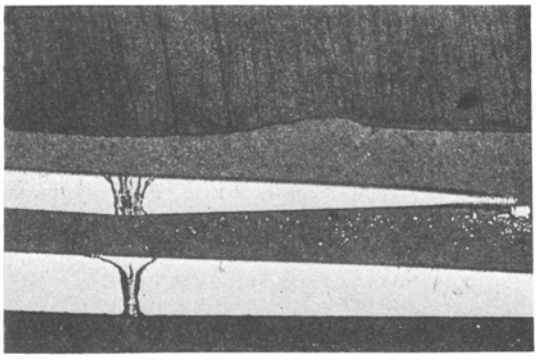

Figure 8 Section through impacted specimen of B-1200 showing broken fibres under the point of impact.

results of Karnes [11], who concluded that this parameter was not speed dependent. This is also the case for the breaking stress of aluminium and A-2024, as thermally activated mechanisms are of little importance in the plastic deformation of these types of material. Fractographic and metallographic observations of the fibres broken under impact (Fig. 8) show that failure occurred in the zone of contact. Fig. 9 shows how the number of broken fibres increases with impact shock. The continuous curves were obtained during slow penetration and the single points represent results from impact tests and indicate the number of fibres broken in each layer as a fraction of the total number of fibres in that layer. The extent of the damage was determined by dissolution of the matrix after the test.

In both the cases considered, slow penetration and impact, the fibres broke predominantly after initiation of a crack on the tensile side of the bent fibre.

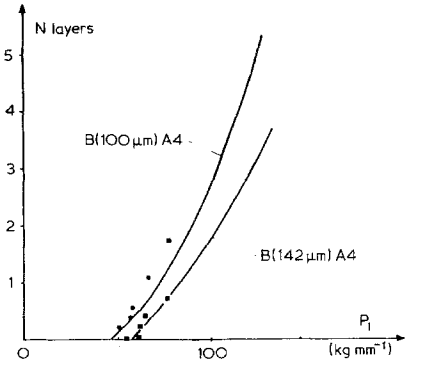

Figure 9 The number of broken fibres in each layer of the B (100 μm) 1200 composite increases as a function of the load applied during slow penetration tests. Punctual results obtained during instrumented impact tests.

The numerical results and the fractographic observations indicate that within the range of speeds available the behaviour of the material under impact is not speed dependent.

5. Residual properties

The tensile strengths of specimens impacted centrally by the cylindrical impacter have been compared to those of similar specimens containing a partial surface notch equivalent in length and width to the damaged zone produced by an impact. This central notch was much wider than the fibre spacing distance but did not interact with the edges of the specimen. The depth of the notch was varied to represent different degrees of damage to the fibre layers. In order to be certain of the damage induced by the slow penetration tests before the residual properties of the specimens were measured X-ray studies of the specimen were made and the development of the damage was monitored by the acoustic emission apparatus.

Several notched specimens in which the notch went completely across the specimen were used to investigate the stress concentration of a notch in the thickness direction. As can be seen in Fig. 10 the strength of the composite was linearly related to the number of layers cut and so showed no notch effect even with only one layer cut. Fig. 11

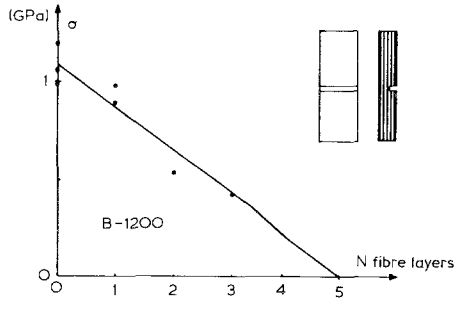

Figure 10 Fibre damage in B (142 μm) 1200 as a function of applied load during slow penetration tests. Punctual results obtained during instrumented impact tests.

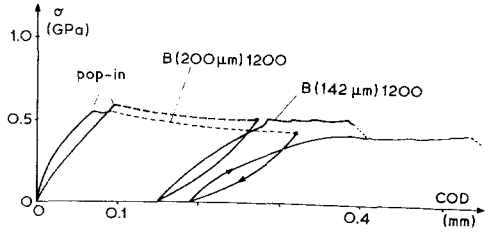

Figure 11 Tensile strength of B-1200 specimens as a function of the notch depth.

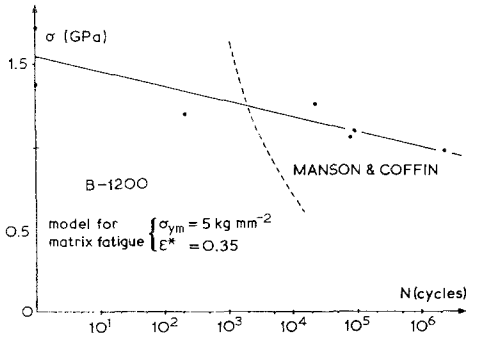

Figure 12 *S–N* curve in cyclic bending for impacted B-1200 ($\sigma_{min}/\sigma_{max} = 0.2$).

shows the similarity of behaviour of the notched and damaged specimens, with both showing unstable crack growth or "pop-in" as revealed by measurement of COD. The pop-in was related to the fracture of the remaining intact material in the impacted or notched zone.

6. Fatigue behaviour

An important part of this study was to determine the course of the accumulation of damage during fatigue loading. For this, both undamaged and impacted specimens have been used. Their geometry was exactly the same as that used for the residual strength properties tests.

All fatigue tests were conducted in circular bending and Figs. 12 and 13 shows the *S–N* curves obtained for undamaged specimens of each type of matrix. The curve shown as a dotted line is the theoretical Manson and Coffin *S–N* curve for the unreinforced matrix material. Three zones can be discerned in the *S–N* curve for the B-2024-T4: (i)

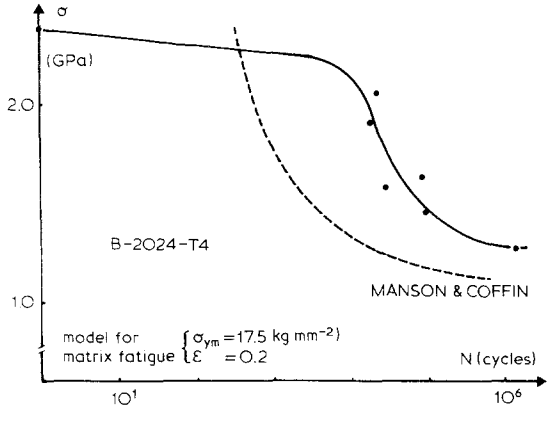

Figure 13 *S–N* curve in cyclic bending for impacted B-2024-T4 ($\sigma_{min}/\sigma_{max} = 0.2$).

a region of quasistatic fracture corresponding to high loads and short lifetimes less than 10^4 cycles during which the behaviour is controlled by the fibres; (ii) an intermediate region during which stress concentrations due to the deformation of the matrix produce fibre failure. The total acoustic emission produced during this period is very limited but reveals the failure of fibres (iii). The AE indicates that the run-out region, which is the third zone, is one in which cracks are developed in the matrix but do not result in the failure of fibres. The structural damage caused by the cracking of the matrix, usually in a direction parallel to the fibres, and the movement of these fracture surfaces produces a great deal of AE.

The S–N curve for the B-1200 specimens was much flatter and does not show the three zones described for the B-2024-T4. This difference is due to the loss of static strength and the lower yield strength of the 1200 matrix, which is unable to transmit such high stress concentrations to the boron fibres.

Figs. 14 and 15 show the S–N curves for both types of impacted specimens with the curves of undamaged specimens shown as dotted lines. The stresses were calculated with respect to the reduced section. Both types of composite show crack growth in the first few cycles during which the matrix bridge in the fibre damaged zone is fractured. In the course of cycling, cracking, both transverse and longitudinal to the fibre direction, has been observed.

For the B-2024 transverse cracking, including fibre failure, occurred over a wide range of cycles and supports the possibility that the stress concentration induced by cracking of the matrix is sufficient to produce failure of the fibres. It can also be seen from Fig. 14 that the effect of the damage becomes of less importance at longer lifetimes as

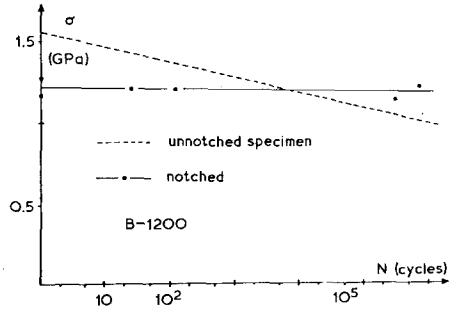

Figure 14 S–N curve in cyclic bending for unnotched B-1200 ($\sigma_{min}/\sigma_{max} = 0.2$).

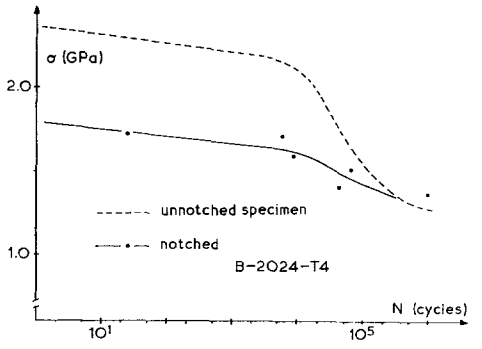

Figure 15 S–N curve in cyclic bending for unnotched B-2024-T4 ($\sigma_{min}/\sigma_{max} = 0.2$).

the curves for the damaged and undamaged specimens converge. This is due to the isolation of the damaged zone by longitudinal cracking parallel to the fibre direction.

The curve for the damaged B-1200 specimen is flat, indicating that the damaged zone is localized and the specimen behaves as though its cross-sectional area had been reduced.

7. Discussion

As has been shown, the importance of an impact and the damage produced is related to the energy of the impact and the resulting fracture of fibres. The fractographic studies have shown that during their fracture the fibres are bent under the point of impact. The matrix, being in a plastic state, is able to accommodate the local deformation without rupturing. If the fibres are considered as beams of stiffer material in a ductile matrix the moment applied to the fibre is given by

$$R = \int_0^{l/2} (\sigma' dx)\, dx \tag{5}$$

where σ' is the stress applied at the surface of the fibre, d is its diameter, and x the distance along the fibre from the point directly under the central point of impact which is the point of maximum turning moment. If l is the distance over which the stress is applied it is possible to write

$$R = \sigma' d \frac{l^2}{8}. \tag{6}$$

The stress σ' is assumed to be a fraction of the stress applied to the composite so that

$$\sigma' = \beta \bar{p} \qquad (\beta < 1) \tag{7}$$

Making use again of Equation 1 we can write

$$R = \frac{2\sigma_f I}{d}$$

and

$$I = \left(\frac{\pi}{4}\right)\frac{d}{2}^4$$

so that

$$R = \frac{\pi d^3 \sigma_f}{32} \quad (8)$$

From Equations 6, 7 and 8

$$\frac{\pi d^2 \sigma_f}{4} = l^2 \beta \bar{p} \, . \quad (9)$$

If the indenter is spherical it is possible to express the applied stress P as

$$P = \bar{p}\frac{\pi l^2}{4} \, . \quad (10)$$

From Equation 10

$$P = \frac{\pi^2}{16}\frac{d^2 \sigma_f}{\beta} \, .$$

For a cylinder, if P_L is the load per unit length of the indenter

$$P_L = \bar{p} l \, .$$

Substituting for l from Equation 9,

$$P_L = \sqrt{\left(\frac{\pi}{4\beta}\sigma_f d_f^2 \bar{p}\right)} \quad (11)$$

Fig. 16 shows that there is a linear relationship between the load corresponding to the first fracture with a spherical indenter and the parameter $\sigma_f d_f^2$. The results in least agreement correspond to the finest fibres used, which were evidently also the most flexible, so that the conditions assumed of rigidity did not apply. Fig. 17 shows that in the case of impact by a cylinder the relationship given by Equation 11 holds. From these curves it can be seen that the values of β are 0.0082 and 0.0077 for the sphere and cylinder respectively.

In determining the residual tensile properties of the impacted specimens it has been shown that there is a linear relationship between COD and the critical transfer length l_c for this type of composite, see Fig. 18. The value of l_c being obtained through the relation $l_c = \sigma_f d/2\tau$. In addition the relationship of $K_c/\sigma d$ to the breaking stress of the fibre is shown in Fig. 19 to be constant, indicating that the tenacity of this material is dependent on the strength of the reinforcing fibres. The tenacity is not dependent on the properties of the matrix, which after impact is not fractured in a direction normal to the broken fibres.

This matrix bridge modifies the stress at the tip of the crack and can be considered as a negative or

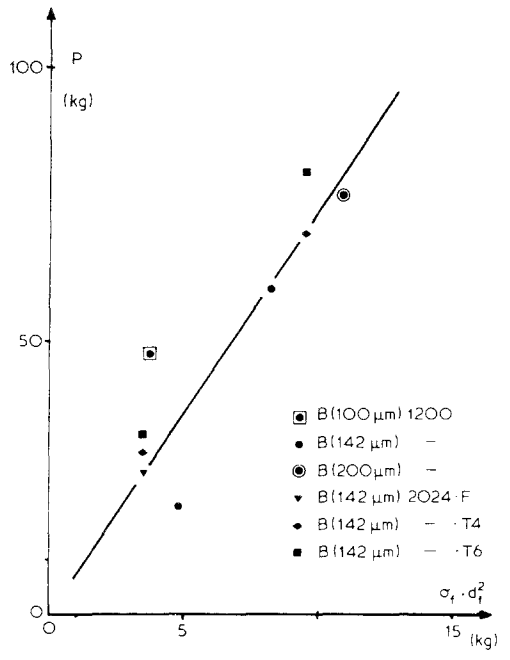

Figure 16 Relationship between the load producing the first fibre failure and $\sigma_f d^2$.

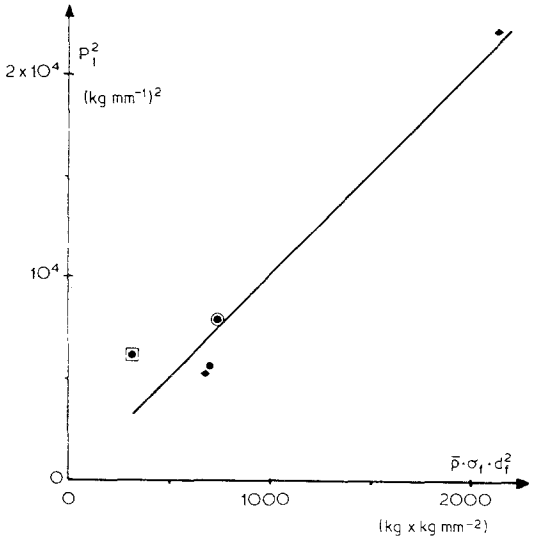

Figure 17 Relationship between the load necessary to produce the first fibre failure and $(\bar{p}\sigma_f d_f^2)$.

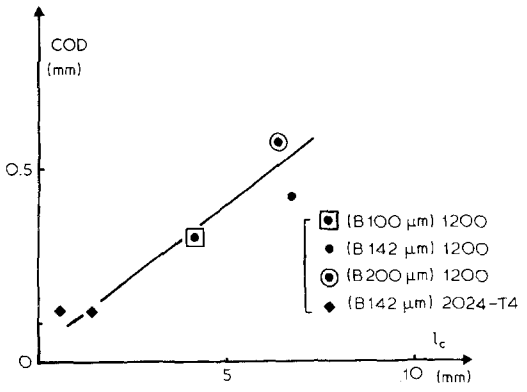

Figure 18 Relationship between COD and the critical load transfer length.

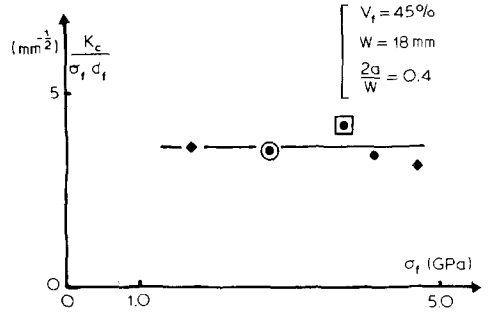

Figure 19 Tenacity of B-Al as a function of the structural parameter.

closing pressure [12]. The stress intensity factor can then be written as

$$K = (\sigma - \sigma') Y\sqrt{a}$$

in which Y is a constant and a the crack length.

From this relationship it is clear that if the breaking stress σ' of the bridging material is less than σ, which is the fracture stress of a centrally notched specimen, failure of the bridge will produce a sudden "pop-in" or extension of the crack without producing a complete failure of the specimen. This type of behaviour was typical of the material tested.

8. Conclusion

This study has demonstrated the failure mechanisms which control the behaviour of boron fibre reinforced aluminium under conditions of impact. The controlling mechanism is the fracture of fibres, which fail predominantly by the bending forces applied through the plastic matrix material. Tensile forces produced by the extension of the fibre as opposed to those produced by bending are greatest at the edge of the contact zone [10]. It is therefore significant that the fibres did not break at the edge of the contact zone but immediately under the impacter at the centre.

The tests, which have covered a wide range of impact speeds, together with the associated analysis have shown that the damage and deterioration produced in the material is described more closely by the product of the fibres breaking stress and their diameter together with the distributed stress on the reinforcing fibres than simply the fracture stress of the composite. The slow penetration test together with the use of the acoustic emission technique is a useful way to study impact properties. In a small number of tests it is possible to obtain all of the damage curve as a function of load and displacement, whereas impact tests are limited to providing isolated results.

The residual tensile properties of impacted boron–aluminium therefore are determined by the intact fibres which remain, and not the matrix material, as we observed no delamination of the matrix parallel to the fibres induced by the impact.

The notch effect for centrally damaged specimens tested in tension was not important and very much larger specimens containing large notches would have to be tested to obtain valid K_c results or K_r curves.

A notch effect in fatigue loading of B-2024-T4 was found for lives less than 10^5 cycles. For longer lifetimes the material showed no notch effect and behaved as in an unnotched state. This was due to the development of longitudinal crack which effectively blocked the extension of the notch.

Acknowledgement

The author would like to thank the D.R.E.T. for their financial assistance for part of this study.

References

1. G. E. HUSMAN, J. M. WHITNEY and J. C. HALPIN, ASTM STP 568 (1974) pp. 92–113.
2. D. W. OPLINGER and J. M. SLEPETZ, ASTM STP 568 (1974) pp. 92–113.
3. B. HARRIS and A. R. BUNSELL, *Composites* 6 (1975) 197.
4. B. R. BUTCHER, *ibid.* 7 (1976) 12.
5. W. J. JACQUES, A.D.-780628 Air Force Institute of Technology, W.P.A.F.B. Ohio (1974).
6. J. G. CARLISLE, A.D.-780612 Air Force Institute of Technology, W.P.A.F.B. Ohio (1974).
7. P. MELNICK and J. Y. TOTH, NASA C.R. 134770 (1975).

8. Y. AWERBUCH and H. T. HAHN, *J. Comp. Mater.* **10** (1976) 231.
9. T. D. GRAY, "Fatigue of Composite Materials" STP 569 (1975) 262-278 ASTM.
10. L. B. GRESZCZUK, ASTM STP 568 (1974) pp. 183–210.
11. M. KARNES, "Mechanical Behaviour of Materials under Dynamic Loads" (Springer Verlag, Berlin, 1968).
12. J. C. LENAIN and A. R. BUNSELL, *J. Mater. Sci.* **14** (1979) 321.

Received 5 December 1978 and accepted 12 March 1979.